Cement & Concrete Composites 33 (2011) 551–561

Contents lists available at ScienceDirect

Cement & Concrete Composites

journal homepage: www.elsevier.com/locate/cemconcomp

Influence of the calcium sulphate source on the hydration mechanism of Portland cement–calcium sulphoaluminate clinker–calcium sulphate binders

Laure Pelletier-Chaignat [a], Frank Winnefeld [a,*], Barbara Lothenbach [a], Gwenn Le Saout [a], Christian Jörg Müller [b], Charlotte Famy [c]

[a] Empa, Swiss Federal Laboratories for Materials Science and Technology, Laboratory for Concrete/Construction Chemistry, Überlandstrasse 129, 8600 Dübendorf, Switzerland
[b] Saint Gobain Weber, Technoramastrasse 9, 8404 Winterthur, Switzerland
[c] Saint Gobain Weber, Rue de Brie, BP84 Servon, 77253 Brie-Comte-Robert, France

ARTICLE INFO

Article history:
Received 25 June 2010
Received in revised form 7 March 2011
Accepted 9 March 2011
Available online 17 March 2011

Keywords:
Calcium sulphoaluminate cement
Calcium sulphate
Pore solution
X-ray amorphous hydrates
Ternary binders

ABSTRACT

Two different binders composed of Portland cement, calcium sulphoaluminate clinker and calcium sulphate were studied from early hydration to 28 days, one containing gypsum and one containing anhydrite at equimolar $CaSO_4$ amount. Sodium gluconate was used as retarder to obtain a sufficient fluidity to cast the samples. Solids were analyzed by X-ray diffraction, scanning electron microscopy and thermogravimetric analysis and quantified by Rietveld refinement, while pore solutions were measured by ion chromatography. Thermodynamic modelling was used to model the hydration process of the ternary binders. This combined study allowed a precise understanding of the hydration process over time and the determination of the composition of the crystalline and of the X-ray amorphous hydrates present in the binders, which cannot be determined by conventional methods. Results show that the hydration mechanisms are similar in presence of gypsum or anhydrite, the difference being in the kinetics of reactions due to the slower dissolution of anhydrite compared to gypsum in the presence of sodium gluconate. The hydration starts with the formation of ettringite and of some X-ray amorphous hydrates. In the anhydrite-bearing system, the ettringite-forming reaction is stronger delayed by the addition of the retarder compared to the gypsum-bearing system. This stronger delay results in the formation of a significant amount of X-ray amorphous hydrates. The hydrates amorphous fraction is composed of different phases and its chemical composition is changing over time. During early hydration, it is mainly composed of aluminium hydroxide and strätlingite, while in the anhydrite-bearing system it can additionally contain some monosulphoaluminate. At later ages, the aluminium hydroxide content decreases and additional monosulphoaluminate and a C-S-H type phase are formed.

1. Introduction

Mortars based on ordinary Portland cement (OPC), calcium sulphoaluminate clinker (CSA) and calcium sulphate can achieve fast setting, rapid hardening and high early strength [1–4], which cannot be reached using OPC-based mortars alone. For those reasons, mortars based on ternary binders represent an interesting alternative for the production of dry-mix mortars. Due to the above mentioned properties, these mortars allow a reduction of working time on the construction sites. Besides this technological advantage, the production of CSA clinker has attracted new interest as it generates lower CO_2 emissions than OPC due to a lower burning temperature in the kiln, a lower CO_2-release from the raw materials (lower calcium carbonate content), and is easy to grind.

The data provided in the literature on the hydration of ternary binders based on OPC, CSA clinker and calcium sulphate, or on similar binders based on laboratory synthesized materials are rare [3–5]. In a previous paper, ternary blends with various OPC/CSA clinker/anhydrite mass ratios were studied, with variable anhydrite contents from 8/3/0.5 to 8/3/1.25, and variable OPC contents from 5/3/1 to 8/3/1 [4]. On the one hand, it was observed that the assemblage of hydrate phases present in the binders after some weeks is not strongly dependent on the changes in the starting ternary composition, and includes ettringite, monosulphoaluminate, hydroxy-AFm (C_4AH_x with x = 13–19 depending on relative humidity), hemicarbonate, strätlingite and a C-S-H type phase (cement notation will be used throughout the text with A: Al_2O_3, C: CaO, F: Fe_2O_3, H: H_2O, M: MgO, S: SiO_2, $\bar{S}$: SO_3, T: TiO_2). Some amorphous/micro-crystalline AH_3 had formed at early age and was later partially consumed during hydroxy-AFm- or monosulphoaluminate-forming reactions. On the other hand, the changes in the

* Corresponding author. Tel.: +41 58 765 45 35.
E-mail address: frank.winnefeld@empa.ch (F. Winnefeld).

0958-9465/$ - see front matter © 2011 Elsevier Ltd. All rights reserved.
doi:10.1016/j.cemconcomp.2011.03.005

starting ternary composition strongly influenced the ettringite to monosulphoaluminate mass ratio.

The modification of the hydration process of OPC or CSA by different quantities or sources of calcium sulphate, such as gypsum, hemihydrate or anhydrite, is well known. In OPC the type and content of calcium sulphate is optimized considering the amount and the reactivity of the aluminate phase (C_3A), in order to form ettringite during early hydration [6]. In pure CSA cements, the hydrate assemblage is not strongly influenced by the amount and type of calcium sulphate added. Ettringite and monosulphoaluminate are formed due to the reaction of ye'elimite ($C_4A_3\bar{S}$) with the calcium sulphate source. However, the amount of added calcium sulphate strongly modifies the ettringite to monosulphoaluminate mass ratio and the water demand to complete full hydration [7–9]. The amount of ettringite is affected by the reactivity of calcium sulphate (solubility and speed of dissolution) at early ages [8]. In ternary binders, the reactivity and speed of dissolution of the calcium sulphate is a key factor for the formation of ettringite or monosulphoaluminate during early hydration [5]. If the reactivity of the calcium sulphate is too low, monosulphoaluminate might form instead of ettringite.

However, there are unsolved issues despite the available data on the hydration mechanism of ternary binders. On the one hand, an important fraction of X-ray amorphous hydrates are present in the binders and their composition is still a matter of debate. AH_3 and a C-S-H type phase are assumed to be part of it, while it could also contain other hydrates not detectable using the X-ray diffraction technique or thermogravimetry (due to overlaps). On the other hand, a previous study showed that the use of an organic retarder is needed to obtain a sufficient workability, and that citric acid efficiently retards the early hydration reactions, such as the ettringite formation, in anhydrite-bearing ternary binders [3,4]. However, the impact of the addition of an organic retarder to CSA-bearing ternary binders based on different calcium sulphate sources has never been described in the literature.

In order to study these topics, two ternary binders based on OPC, CSA clinker and gypsum or anhydrite were examined in the presence of sodium gluconate ($NaC_6H_{11}O_7$). To obtain the quantitative composition of the solid phase, the hydrated binders were studied by X-ray diffraction (XRD)/Rietveld refinement and thermogravimetric analysis (TGA). The liquid phase was studied by ion chromatography (IC), pH and total organic carbon measurements in order to follow the chemical evolution of the pore solution over time and to evaluate the adsorption of the gluconate on the cement particles or hydrate phases. Based on the obtained analytical data, thermodynamic modelling was used to calculate the effective saturation indices and to simulate the evolution of the solid and liquid phases over time. These thermodynamic calculations coupled to analytical data allowed a better understanding of the hydration mechanism and of the nature of the hydrates amorphous fraction present in the ternary binders.

2. Materials

The chemical and mineralogical compositions of the raw materials can be found in Table 1. The chemical composition was measured by X-ray fluorescence (XRF), except for sulphur which was determined with a Leco® apparatus. Free lime content was measured according to Franke [10]. The mineralogical composition was determined from the X-ray diffraction (XRD) patterns using Rietveld refinement. The OPC used was an OPC CEM I 52.5 R containing 3.5% anhydrite and 0.9% hemihydrate. Its free lime content was measured to be 0.25% and its Blaine fineness at 5030 cm^2/g. The CSA clinker used contained 62.8% ye'elimite ($C_4A_3\bar{S}$) and was characterized by CA and CA_2 present as minor hydraulic components, 8.1% and 3.1% respectively. It had a Blaine fineness of 4180 cm^2/g. Both calcium sulphates used were technical products. The gypsum contained some anhydrite (3.3%) and the anhydrite some SiO_2 (1.1%). To determine the amount of alkali sulphates in the OPC and in the CSA clinker (K_2SO_4 and Na_2SO_4 in Table 1), 5 g of cement or clinker were stirred in 50 ml of deionised water for 5 min. Solution was then filtered and Na and K concentrations in solution were measured by ion chromatography. The selected ternary gypsum- and anhydrite-bearing formulations (TER-G, TER-A) were chosen to have the same total SO_3 content (Table 1).

3. Methods

All the experiments were performed at 20 °C and at a water to cement ratio of 0.42. For each sample, 900 g of cement were mixed with 378 g of deionised water according to the EN 196-3 standard. The pastes were cast in 500 ml polyethylene (PE) bottles, sealed and stored in a thermostatic water bath. The increase of temperature during the first hours of hydration was measured for TER-G in the centre of the bottle to check whether the temperature increase was relevant. The temperature reached about 23.5 °C after 3 h, and then quickly decreased to about 20.0 °C. The conditions were nearly isothermal. The pore solutions were extracted after 1 h, 5 h 30, 15 h 30, 1 day, 7 days and 28 days. Unset samples were pressure filtered to separate the solid and liquid phases (TER-G at 1 h, TER-A at 1 h and 5 h 30), while the hardened samples were treated with the steel die method to extract the pore solutions [11]. A maximum pressure of 250 N/mm^2 was used to extract the pore solutions from hardened pastes.

With a syringe equipped with a Nylon filter 0.45 μm, 4.5 ml of the liquid phase of each sample were immediately collected and placed into separate vessels. In the first PE-vessel 1 ml of solution was diluted (1:10) with Milli-Q water for ion chromatography. The second PE-vessel was filled with 3 ml of solution to determine the pH value. A 35 ml glass vessel was filled with 0.35 ml of pore solution and diluted (1:10) with Milli-Q water for total organic carbon (TOC) measurement. To determine the pH value, a Knick SE pH/Pt1000 electrode was used. In order to minimize the alkali error, fresh KOH solutions with known concentration were measured (0.001 mol/l to 1 mol/l). The obtained values were correlated to the calculated ones, considering the temperature during measurement (~23 °C) and the ionic strength of the KOH solutions. The total concentrations of Al, Ca, Na, K, Si and S were determined using ion chromatography (Dionex ICS-3000). The total organic content (TOC) of the pore solution samples was measured using a Sievers 5310C.

Heat flow curves were obtained by isothermal calorimetry with a Thermometric TAM Air instrument calibrated at 600 mW, in order to obtain an overview of the hydration kinetics of the two ternary binders. For the analysis, about 3.4 g of paste were mixed inside the apparatus using the admix ampoules [12].

X-ray diffraction (XRD) and thermogravimetry (TGA) were used to determine the mineralogical composition of the solid phase. Prior to the analyses, hydration was stopped by plunging the samples 1 h in about 50 ml isopropanol and rinsing twice with diethylether. Samples were subsequently dried in a desiccator for about 12 h at room temperature. Prior to XRD and TGA, cement was ground to a grain size <63 μm for the analysis. The thermogravimetric analyses were done with a Mettler Toledo TGA/SDTA851e, where about 10 mg of sample were placed in an open vessel under N_2 atmosphere, heating up 20 °C/min up to 980 °C.

XRD data were collected using a PANalytical X'Pert Pro MPD diffractometer in a θ–2θ configuration using incident beam monochromator employing the Cu Kα radiation (λ = 1.54 Å) with a fixed divergence slit 1° and a rotating sample stage. The samples were

Table 1
Mineralogical and chemical compositions of the used materials and used formulations.

	OPC (wt.%)	CSA (wt.%)	$C\bar{S}H_2$ (wt.%)	$C\bar{S}$ (wt.%)		OPC (wt.%)	CSA (wt.%)	$C\bar{S}H_2$ (wt.%)	$C\bar{S}$ (wt.%)		TER-G (g)	TER-A (g)
$C_4A_3\bar{S}$		62.8			SiO_2	22.7	4.5		1.0	OPC	61.5	61.5
CT		5.7			Al_2O_3	3.7	45.0		0.4	CSA	26.7	26.7
C_2AS		18.3			Fe_2O_3	1.4	1.5		0.4	$C\bar{S}H_2$	10.7	
CA		8.1			CaO	64.9	36.1	33.3	40.2	$C\bar{S}$		8.4
CA_2		3.1			Na_2O	0.20*	0.07*					
MA		1.8			K_2O	0.70*	0.35*			w/c	0.42	0.42
C_3S	64.1				MgO	0.80	0.91	0.29	0.10			
C_2S	19.0				SO_3	3.2	8.6	46.7	55.6			
C_4AF	1.9				TiO_2	0.18	2.23					
C_3A	7.7				P_2O_5	0.14	0.08					
$C\bar{S}$	3.5		3.3	98.8	Mn_2O_3	0.05	0.02					
$C\bar{S}H_{0.5}$	0.90				SrO	0.18	0.09					
$C\bar{S}H_2$			96.7		Cl	0.03	<0.01					
K_2SO_4	0.71	0.06			L.O.I.	1.8	0.7	21.5	1.4			
Na_2SO_4	0.081	0.005										
CaO (free)	0.25	0.01										
MgO		0.20										
SiO_2	0.60			1.1								
$CaCO_3$	2.3											

Mineralogical composition determined by XRD/Rietveld refinement. Chemical analyses by XRF, except for SO_3 measured with a Leco® apparatus. CaO (free) determined according to Franke [10]. Loss on ignition (L.O.I) measured until 950 °C. *: Na_2O and K_2O contents measured by SEM/EDX are 0.39 ± 0.24 wt.% and 0.6 ± 0.2 wt.% in C_3S, 0.15 ± 0.02 wt.% and 0.8 ± 0.3 wt.% in CA_2 and 0.24 ± 0.01 wt.% and 0.2 ± 0.1 wt.% in CA. K_2O content of $C_4A_3\bar{S}$ was measured at 0.6 ± 0.3 wt.%.

scanned between 5° and 80° with the X'celerator detector. The anhydrous OPC was analyzed according to the protocol presented by Le Saout et al. [13] with the X'Pert High Score Plus 2.1 from PANalytical. The phases used for the Rietveld refinement of the CSA clinker and the ICSD codes (Inorganic Crystal Structure Database, web version 1.1.0) of the structural data are given in Table 2.

Once the refinements of the raw materials had been done, the unit cell dimensions and shape parameters of the anhydrous phases were kept constant during the refinement of the diffractogram of the hydrated pastes. The presence in the hydrated pastes of some ill crystallized phases required an internal standard for quantification [21 and references therein]. On that purpose, a known quantity of an internal standard CaF_2 (around 10 wt.%) had been added to the mixtures and the entire pattern had been fitted using the Rietveld method. The analyses were then corrected by dividing the values obtained by Rietveld by the ratio of the measured to true amount of standard. The difference between the sum of the corrected weight fractions of the crystalline components and 1 was assumed to represent the total weight fractions of the unknown or X-ray amorphous hydrates. This amorphous fraction of hydrates includes all the amorphous and/or micro-, nano-crystalline components that are not detectable using the XRD technique. Results of Rietveld analyses gave the sum of the phases normalized to 100 wt.%. Due to hydration reactions, water entered the solid system and the amount of anhydrous phases decreased with time by the effect of dilution. In order to avoid this apparent dilution effect, the water content of the sample was deduced using the TGA results, so that the results were referred to the mass of anhydrous materials. The total could therefore be $\geqslant$100 wt.% (at w/c = 0.42, maximum is 142 wt.% representing 100 g of dry cement mixed with 42 g of water if all the water is incorporated in the system). The final result was then normalized to 100% (g/100 g paste). With this data representation, the "real" decrease or increase of the various phases can be observed. The error from the Rietveld refinement ranges between 5% and 20% for the clinker phases, while for the calcium sulphates it can go up to 40%.

Table 2
ICSD codes used for the Rietveld refinement.

Phases	Formulae	Crystal system	ICSD	References
Ye'elimite	$Ca_4Al_6O_{12}SO_4$	Orthorhombic	80361	[14]
		Cubic	9560	[15]
Gehlenite	$Ca_2Al_2O_5SiO_2$	Tetragonal	67687	[16]
Calcium monoaluminate	$CaAl_2O_4$	Monoclinic	260	[17]
Calcium dialuminate	$CaAl_4O_7$	Monoclinic	16191	[18]
Perovskite	$CaOTiO_2$	Orthorhombic	62149	[19]
Spinel	$MgAl_2O_4$	Cubic	77583	[20]

Energy-dispersive X-ray spectroscopic (EDX) analyses were performed at the scanning electron microscope (SEM) in order to determine the chemical composition of the main clinker phases from the OPC and CSA clinkers, and to gain information on the CaO content of some hydrates. The microscope was operated at 15 kV in the backscattered electron mode to select the positions of the EDX analyses during which major and minor elements were semi-quantitatively measured (Ca, Al, Si, S, Fe, Mg, Ti, Na, K, Zn and Cr).

A mass balance calculation was used to determine the CaO, Al_2O_3, SO_3 and SiO_2 contents of the X-ray amorphous fraction of the hydrated pastes. In the one hand, the contents of the various oxides in the whole system were calculated using the chemical composition of the OPC, the CSA clinker and the calcium sulphates. In the other hand, the contents of the various oxides in the crystalline phases (anhydrous and hydrates) and their increase or decrease observed by Rietveld refinement were considered. Chemical composition of C_3S, $C_4A_3\bar{S}$, CA, C_2AS and CT were measured by EDX on the anhydrous clinkers, while the chemical composition of the anhydrite and gypsum were known. For C_3A, C_2S and C_4AF, values were taken from Taylor [22]. For calcite, quartz, spinel (MA), ettringite and portlandite, oxides contents were calculated from their theoretical stoechiometry, the two lasts being too small to be separately measured by EDX. Finally, the chemical composition of all the crystalline solids was deduced from the total composition of the system for each oxide, giving the composition of the amorphous fraction for this oxide.

In order to carry out the thermodynamic calculations, the geochemical GEMS-PSI software was used linked to the cement-specific CEMDATA database [23–27]. Thermodynamic modelling was used to calculate the saturation indices of the various hydrate phases which could potentially form in the hydrating binder, using

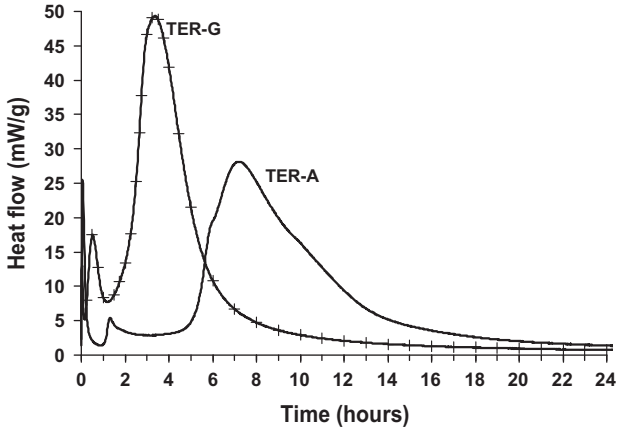

Fig. 1. Heat flow curves obtained by isothermal calorimetry on the gypsum-bearing (TER-G) and on the anhydrite-bearing (TER-A) systems during the first 24 h of hydration.

the composition of the pore solutions. This shows when and which hydrates were in equilibrium with the pore solution, thus being able to precipitate. When the pore solution is undersaturated with respect to a certain solid, it is not formed. Thermodynamic calculations were also carried out to model the hydration processes of the two studied ternary binders over time. The following modelling strategy was applied: (i) The chemical compositions of the two dry-mixed cements were used as input, (ii) the dissolution kinetics determined from XRD/Rietveld refinement for C_3S, C_2S, C_4AF, C_3A, $C_4A_3\bar{S}$, CA, $CaCO_3$, $C\bar{S}H_2$ and $C\bar{S}$ were fitted using polynomial equations, while K_2SO_4, Na_2SO_4, hemihydrate, free MgO and free lime were allowed to dissolve instantaneously and spinel (MA), quartz, perovskite (CT), gehlenite (C_2AS) were considered to be inert (based on the XRD data), and (iii) the thermodynamic equilibria for the solid phases involved in the hydration process were calculated by GEMS considering the given empirical dissolution kinetics mentioned above. As no dissolution kinetics could be provided for CA_2 by the Rietveld refinement due to its low amount (<1 wt.%) in the ternary blends and to peak overlap, the dissolution of CA was used to model the CA_2 decrease (the same empirical equation was used). Free MgO was allowed to dissolve instantaneously due to its very low concentration in the two ternary binders (<0.06 wt.%), which did not strongly influence the modelled hydration process.

4. Results and discussion

In the absence of an organic retarder TER-G and TER-A set within some minutes. However, in the presence of sodium gluconate, TER-A is more retarded than TER-G. This is clearly visible on the heat flow calorimetric curves (Fig. 1). TER-G heat flow curve shows two peaks, the first one has a maximum heat flow around 30 min and the second one around 3 h. In TER-A two similar peaks are observed and delayed. The first peak has a maximum heat flow

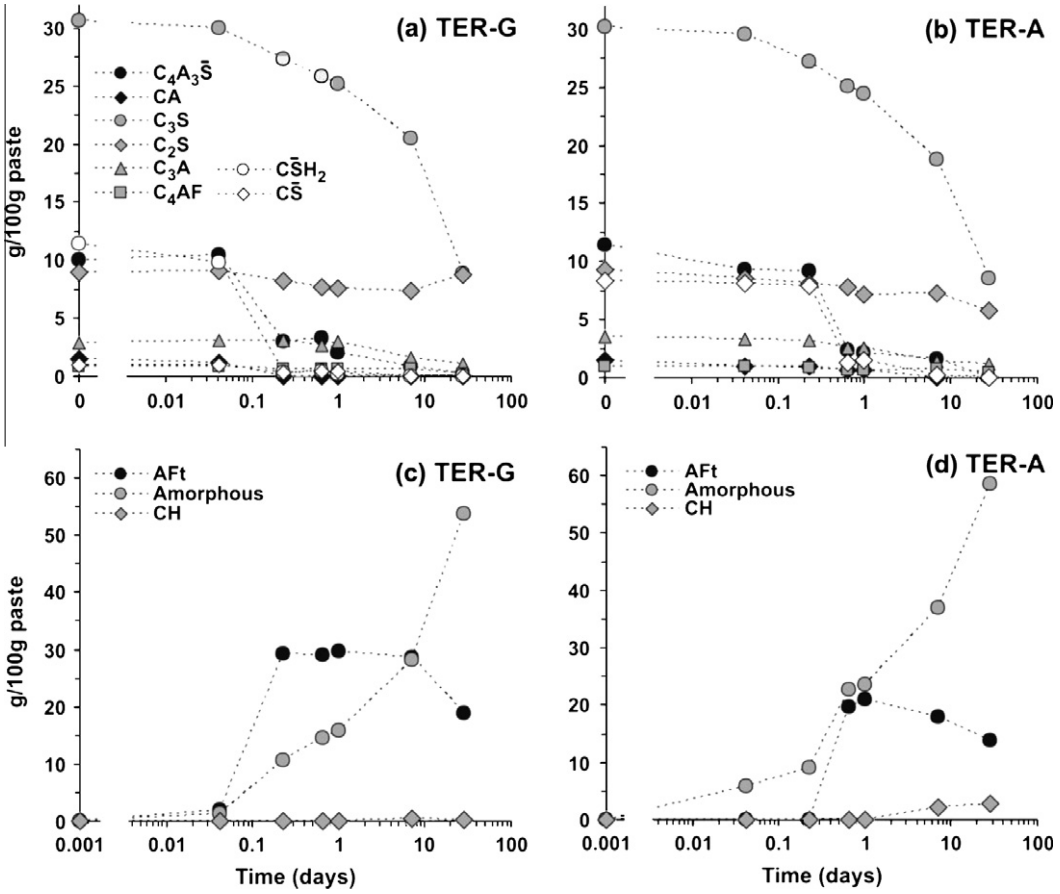

Fig. 2. Evolution of the solid phase composition over time deduced from X-ray diffraction, Rietveld refinement and thermogravimetry for the gypsum-bearing (TER-G) and the anhydrite-bearing (TER-A) systems: (a and b) consumption of clinker phases and calcium sulphates, (c and d) formation of hydrate phases. AFt = ettringite, Amorphous = X-ray amorphous hydrates, CA = monocalcium aluminate, C_3A = aluminate, C_4AF = ferrite, $C_4A_3\bar{S}$ = ye'elimite, CH = portlandite, C_3S = alite, C_2S = belite, $C\bar{S}$ = anhydrite, $C\bar{S}H_2$ = gypsum. The amount of solid is presented as g/100 g of paste in order to avoid artefacts due to "dilution" effects (see methods description above).

around 1 h 30 and the second one around 7 h. However, the second peak seems to be composed of several convoluted peaks (shoulders at 6 h and 10 h), suggesting a more complex hydration evolution than TER-G at early ages with the formation and conversion of hydrates. The following paragraphs will always refer to the retarded mixes.

4.1. Solid phase composition

In TER-G, the Rietveld refinement analysis reveals that within the first hour only the rapid soluble phases of the OPC are dissolved such as the soluble alkalis (K_2SO_4 and Na_2SO_4), free lime (CaO_f) and hemihydrate. Only little C_3S dissolves within these first hours (Fig. 2a and c), and continues to dissolve until later ages. According to the Rietveld result, almost no or very little $C_4A_3\overline{S}$ seems to dissolve within the first hour (considering an error of 20% for $C_4A_3\overline{S}$). The period between 1 h and 5 h 30 is characterized by a strong decrease in the $C_4A_3\overline{S}$ content and the complete consumption of the gypsum ($C\overline{S}H_2$). This leads to the massive formation of ettringite (AFt) due to the reaction (i) $C_4A_3\overline{S} + 2C\overline{S}H_2 + 34H \rightarrow C_3A{\cdot}3C\overline{S}{\cdot}H_{32} + 2AH_3$, and of some X-ray amorphous hydrates (Fig. 2c). From 5 h 30 to 7 days, $C_4A_3\overline{S}$ is dissolving in the absence of gypsum. The AFt content stays constant, while the amount of X-ray amorphous hydrates strongly increases. The period beyond 7 days is characterized by a decrease of the AFt content, while some X-ray amorphous hydrates are still formed.

The hydrate phases observed in the derivative TGA curves for TER-G (Fig. 3a) are partly in agreement with the XRD results, including AFt and some X-ray amorphous hydrates, while monosulphoaluminate is additionally found in the TGA curves at hydration times of 7 and 28 days due to the reaction (ii) $C_4A_3\overline{S} + 18H \rightarrow C_3A{\cdot}C\overline{S}{\cdot}H_{12} + 2AH_3$. A little amount of CH seems to be present in the samples at 7 day and 28 day. The formation of AFt starts within the first hour. In order to be able to form AFt, it is obvious that some $C_4A_3\overline{S}$ or C_3A had dissolved at that time, in contrast to what was shown by Rietveld refinement. This discrepancy is due to the uncertainty of the Rietveld refinement method, which could be around ±2 g for 10 g of $C_4A_3\overline{S}$ (difference between $C_4A_3\overline{S}$ in the dry mix and the corresponding Rietveld result for the same sample). Even if the presence of some X-ray amorphous hydrates is deduced from the derivative TGA curves, their nature cannot be precisely determined using this method. The corresponding broad and flat peak ranges between 200 °C and 400 °C and could therefore be related to the presence of some AH_3, which would be in agreement with the AFt-forming reaction (i) mentioned above. However, AH_3 is probably not the only phase responsible for this signal. Moreover some additional peaks related to some X-ray amorphous hydrates (e.g. a C-S-H type phase) could be present at temperatures <200 °C overlapping with AFt and/or monosulphoaluminate.

More information can be gained from a mass balance calculation based on the XRD data to estimate the CaO, Al_2O_3, SO_3 and SiO_2 contents in the hydrates amorphous fraction, and its elemental molar ratios (Fig. 4a and c). In TER-G at 1 h, about 12% of the total Al_2O_3 of the system and no or little SiO_2 or SO_3 are present in the amorphous fraction. This confirms that some AH_3 forms in TER-G within the first hour. Beyond 1 h, some SiO_2 and SO_3 are contained in the amorphous fraction, showing that AFm-type phase(s) and/or a C-S-H type phase could be present in it. The decrease over time of the calculated Al to Si molar ratio in the amorphous fraction is in agreement with the consumption of AH_3 and the formation of a C-S-H type phase during late hydration reactions observed in similar ternary binders [4].

In TER-A the kinetics of clinker dissolution and hydrate phases formation is different to the one of TER-G, except for the rapid dissolution of the alkali sulphates (K_2SO_4 and Na_2SO_4), free lime (CaO_f) and hemihydrate during very early hydration. Until 5 h 30, C_3S is the main phase to react and the volume of the X-ray amorphous fraction increases (Fig. 2b and d). As for TER-G, C_3S continuously dissolves in the investigated samples over time. The massive consumption of $C_4A_3\overline{S}$ and anhydrite occurs later compared to TER-G, between 5 h 30 and 1 d, leading to the massive formation of AFt (Fig. 2d) via the reaction (i) $C_4A_3\overline{S} + 2C\overline{S} + 38H \rightarrow C_3A{\cdot}3C\overline{S}{\cdot}H_{32} + 2AH_3$. The decrease of the AFt content starts beyond 1 day and is coupled to the formation of some X-ray amorphous hydrates. Some CH is present in TER-A at 7 day and 28 day (Fig. 2d). From the Rietveld refinement analysis, less AFt and more amorphous hydrates and CH form in TER-A compared to TER-G.

The hydrate phases observed in the derivative TGA curves of TER-A are partly in agreement with the XRD results (Fig. 3b), including AFt and some X-ray amorphous hydrates, while monosulphoaluminate is additionally found in the TGA curves. As previously mentioned, the composition of the hydrates amorphous fraction cannot be gained from the derivative TGA curves. However, the mass balance calculation shows that some CaO, Al_2O_3, SO_3 and SiO_2 are present in the amorphous fraction from the early hydration period (Fig. 4b). It could therefore contain some monosulphoaluminate and other AFm-type phases or a C-S-H type phase. The mass balance calculations showed that the composition of the hydrates amorphous fraction in TER-A is slightly modified within the first hours of hydration, compared to TER-G where it is more significantly changed with a strong decrease of the Al to Si ratio (Fig. 4c and d).

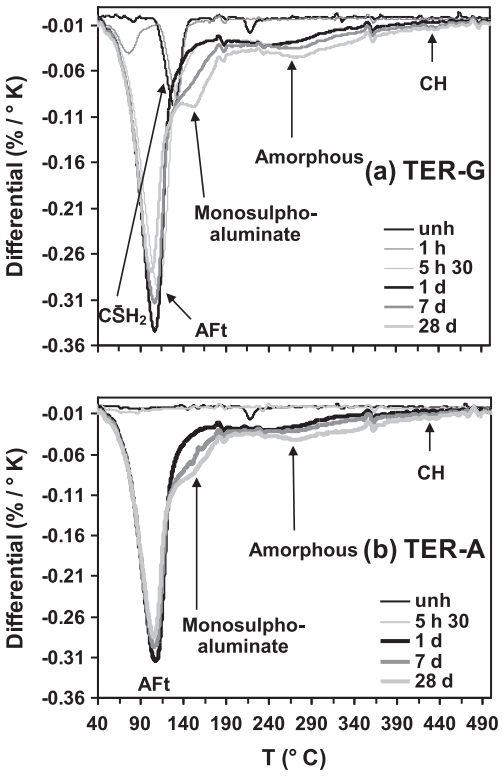

Fig. 3. Selected derivative curves from the thermogravimetric analyses for a) the gypsum-bearing system (TER-G) and b) the anhydrite-bearing system (TER-A). The peak around 215 °C in the unhydrated mixes is related to the sodium gluconate. The following curves were omitted for readability: TER-G at 15 h 30 (equal to 1 d), TER-A at 1 h (similar to 5 h 30) and TER-A at 15 h 30 (similar to 1 d). AFt = ettringite, Amorphous = partial signal related to the X-ray amorphous hydrates (part of the signal probably overlaps with AFt or monosulphoaluminate at lower temperature and is therefore not visible), $C\overline{S}H_2$ = gypsum. Monosulphoaluminate is an SO_4–OH–monosulphate solid solution close to $C_4A\overline{S}H_{12}$.

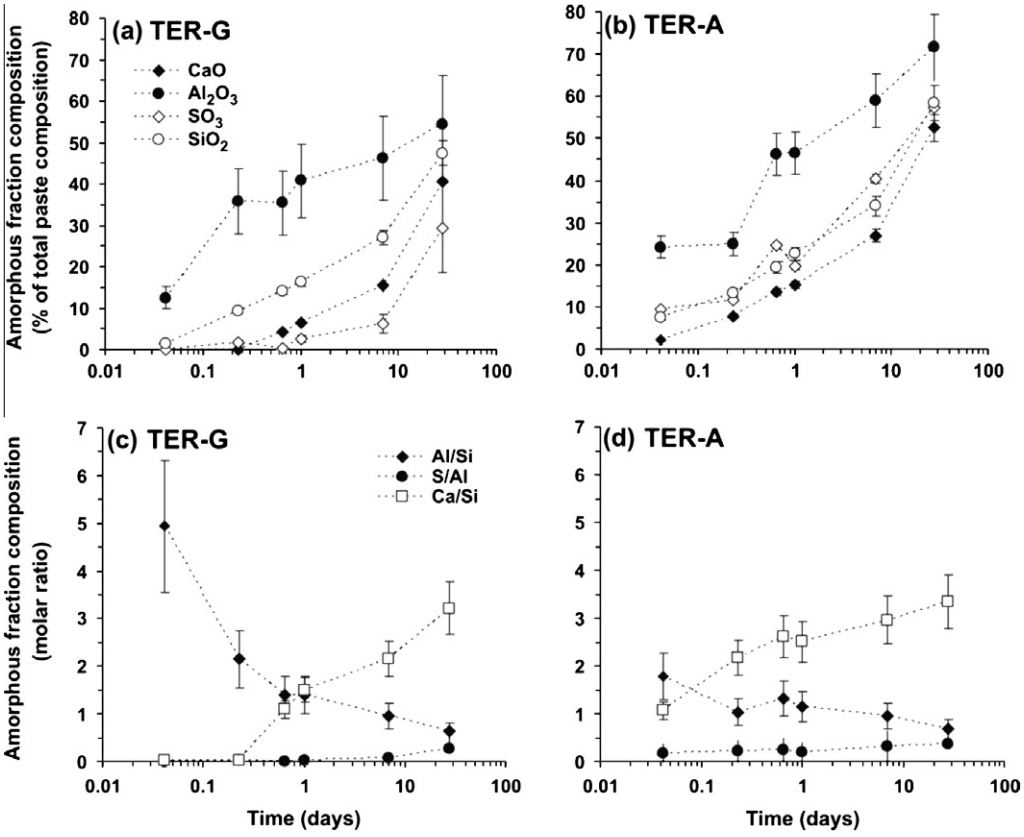

Fig. 4. Estimation of the composition of the hydrates amorphous fraction deduced from mass balance calculations. CaO, Al_2O_3, SO_3 and SiO_2 contents compared to the composition of the whole system (total paste composition) in (a) the gypsum-bearing system (TER-G) and (b) the anhydrite-bearing system (TER-A) and elemental molar ratios in the hydrates amorphous fraction in (c) the gypsum-bearing system (TER-G) and (d) the anhydrite-bearing system (TER-A). Error bars are based on the calculated uncertainty between the theoretical mix composition and the Rietveld refinement calculated composition of the ternary dry mixes, and on the error related to the TGA method (including error propagation during calculation).

4.2. Liquid composition

All results obtained from the chemical analyses of the extracted pore solutions, including elemental compositions, pH and total organic carbon measurements, are presented in Table 3. In pore solutions from TER-G and TER-A, Na and K continuously increase over time (Fig. 5a and b). They are released by the alkali sulphates (Na_2SO_4 and K_2SO_4) and sodium gluconate (only Na) at the early beginning and later by the dissolution of the clinker phases [11,22,28,29], such as C_3S and C_3A from the OPC or $C_4A_3\bar{S}$, CA_2 or CA from the CSA clinker (see Na_2O and K_2O contents measured in these phases by SEM/EDX; footnote of Table 1).

In order to be able to evaluate an eventual alkali uptake by the hydrate phases, the discrepancy between the calculated and the measured contents of alkalis in the pore solution was determined (Fig. 6), taking into account only the measured dissolution of the clinkers, of the easily soluble alkali sulphates and of the sodium gluconate. The calculated and measured curves generally evolve in a parallel way, showing that alkalis are hardly incorporated into hydrate phases and that their increase in solution is mainly related to their release from the clinker phases and to the decrease of the pore solution volume over time. In TER-G the calculated values tend to be overestimated between 1 h and 5 h 30, when AFt and some X-ray amorphous hydrates are formed. Some small

Table 3
Measured total concentrations in the pore solutions from the ternary binders (w/c = 0.42).

Sample	Time (days)	pH	Al (mmol/l)	Na (mmol/l)	K (mmol/l)	Ca (mmol/l)	Si (mmol/l)	S (mmol/l)	OH (mmol/l)	TOC (mmol/l)
TER-G	0.04	11.98	4.3	319	124	6.5	0.06	226	10	25
	0.2	12.41	5.1	385	188	1.2	0.13	146	28	30
	0.6	13.04	5.5	392	202	0.9	0.27	37	120	28
	1	13.06	5.5	406	215	0.7	0.26	36	125	30
	7	13.61	5.0	525	274	0.8	1.67	13	446	37
	28	n.e.	3.7	795	551	1.2	1.28	13	n.e.	n.e.
TER-A	0.04	12.55	7.5	314	123	23.0	0.14	143	39	80
	0.2	12.57	5.0	316	124	27.8	0.05	150	41	96
	0.6	12.31	4.6	505	249	1.9	0.15	277	22	38
	1	13.06	6.1	528	273	3.0	0.47	129	125	44
	7	13.65	5.5	687	384	0.6	2.61	29	485	47
	28	13.84	3.6	933	657	1.4	1.87	42	760	n.e.

TOC: total organic carbon, n.e.: not sufficient pore solution to perform measurement.

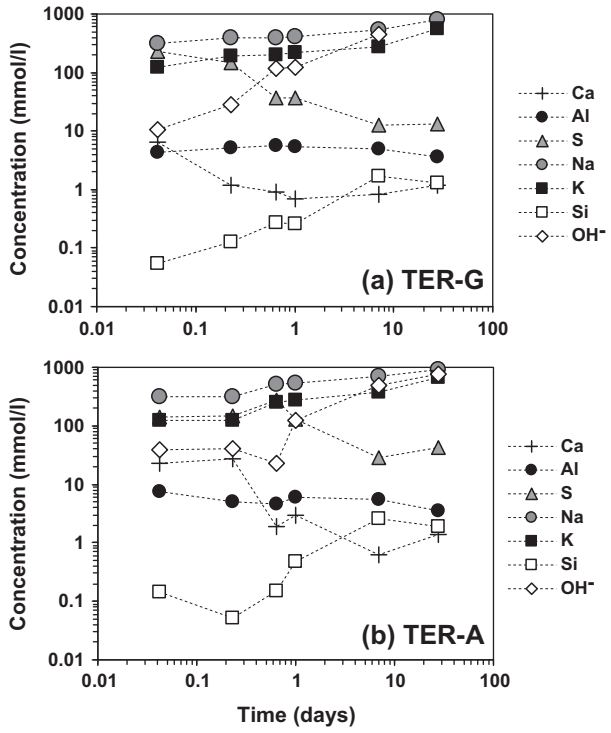

Fig. 5. Total concentrations of major elements measured in the pore solutions in (a) the gypsum-bearing system and (b) the anhydrite-bearing system. No OH^- value is presented for TER-G at 28 days, because not enough pore solution was extracted to allow pH measurement.

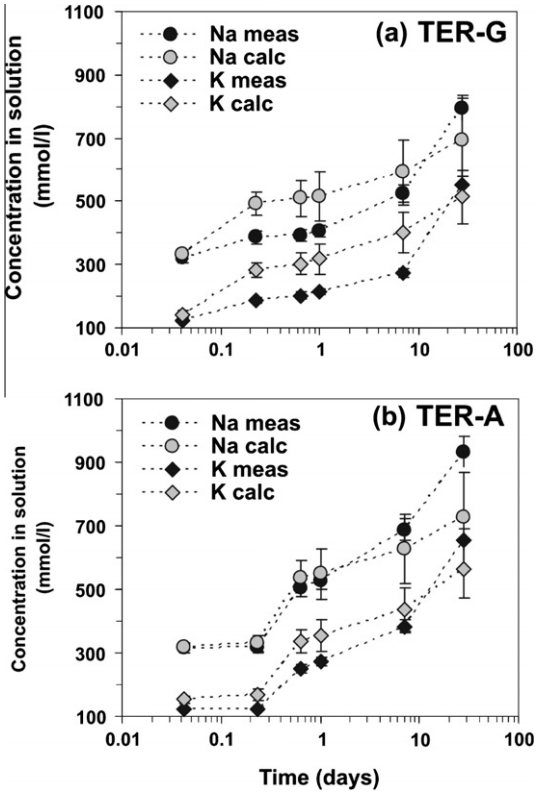

Fig. 6. Measured (meas) and calculated (calc) total concentrations of Na and K in pore solutions: (a) in the gypsum-bearing system (TER-G) and (b) in the anhydrite-bearing system (TER-A). The calculated curves were obtained considering an instantaneous dissolution of the alkali sulphates from the OPC and CSA clinkers, the release of Na from the sodium gluconate, and no uptake of alkalis by the forming hydrate phases. The release of Na and K from clinker phases over time was estimated from the Rietveld refinement results (dissolution kinetics) and from the energy-dispersive X-ray spectroscopic analyses (Na_2O and K_2O contents in the clinker phases) obtained at the scanning electron microscope. Error propagation was calculated considering errors of 1% for the TGA, 5% for the IC and 0.1% for the EDX analyses.

quantities of alkalis could therefore be sorbed by one or more of these phases. According to Andac and Glasser [30], some K can be sorbed by hydrates during the hydration of CSA cements beyond 3 days when monosulphoaluminate and strätlingite are formed. Moreover, strätlingite was clearly identified to be a K-binding phase in CSA cements [29]. Other literature data obtained on synthetic gels, such as C-S-H, C-A-S-H or M-S-H, showed that Na and K can be sorbed by these gels [31–34].

The Ca and S concentrations tend to decrease over time in the pore solutions of TER-G and TER-A (Fig. 5). They are released by the dissolution of $C_4A_3\bar{S}$, of the calcium sulphates, and Ca is additionally released during free lime and OPC clinker dissolution. As soon as they are released in solution, they are consumed to form the AFt and some X-ray amorphous hydrates. Some SEM/EDX analyses showed that the hydrates amorphous fraction contains some Ca, which was confirmed by the mass balance calculations on the solid phases.

The Al concentration in the solutions stays constant in TER-G and TER-A (Fig. 5). It is balanced by the $C_4A_3\bar{S}$ dissolution, and the formation of AFt and of some Al-bearing amorphous hydrates. The dissolved Si concentration in TER-G continuously increases until 7 days (Fig. 5a). It is released by the dissolution of C_3S/C_2S and is incorporated in the hydrates amorphous fraction (Fig. 4a). Between 7 and 28 days, the dissolved Si concentration is rather constant (Fig. 5a). This could be due to the formation of some Si-bearing phases in the amorphous fraction, such a C-S-H type phase or an AFm-type phase. The evolution of the Si contents in pore solutions from TER-A is similar to the one observed in TER-G.

The evolution of the OH^- concentration in solution is negatively correlated to the S concentration and positively correlated to the Na and K concentrations, as the charge balance of the solution is maintained. For that reason OH^- generally increases over time in both TER-G and TER-A (Fig. 5). During early hydration pH values are lower than 12.6, being similar to pH values observed in the pore solutions of CSA cements [29]. At later ages they range between 13 and 14, being similar to pH values observed in pore solutions of OPC [11,26,28,35].

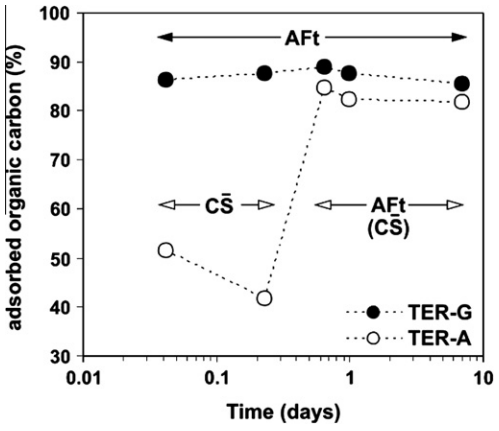

Fig. 7. Percentage of adsorbed organic carbon calculated from the total organic carbon measurement of the pore solutions in the gypsum-bearing system (TER-G) and the anhydrite-bearing system (TER-A). AFt = ettringite, $C\bar{S}$ = anhydrite.

The measurement of the total organic carbon concentration in solution reveals that in TER-G, the percentage of adsorbed organic

carbon reaches about 85% after 1 h and then stays constant (Fig. 7). This means that 15% of the added gluconate stay in the pore solution until 28 days, whereas 85% are adsorbed. In TER-A, it is below 50% until 5 h 30 and then increases to about 83% and stays constant. From Fig. 2, it can be deduced that the samples, where the percentage of adsorbed organic carbon is higher than 80%, are those containing relevant amounts of AFt and/or gypsum (TER-G at 1 h). According to literature data, AFt in natural or synthesized pore solutions can adsorb high amounts of negatively charged polycarboxylate-based superplasticizers [36–39]. As the gluconate used in the present study is also negatively charged, it could adsorb on AFt surfaces. According to Zingg et al. [39–40] the number of submicron particles, which are mainly AFt in OPC, is much higher in cement paste at early age than in unhydrated cement. Therefore the high specific surface area of AFt could be available for the gluconate to adsorb, and could explain the high percentage of adsorbed organic carbon observed in TER-G at 1 h. In TER-A within the first hours, lower amounts of organic carbon are adsorbed, about 50%, while AFt is not present in the pastes. In that case, the gluconate could adsorb on another phase having a strongly positive zeta potential in pore solution such as e.g. an AFm-type phase [36,38], which could be present in the hydrates amorphous fraction of TER-A at early age as shown by the mass balance calculations (Fig. 4b).

4.3. Thermodynamic modelling

4.3.1. Saturation indices

The effective saturation index shows which hydrates are in equilibrium with the pore solution (saturation index = 0), or are oversaturated (saturation index > 0), thus being able to precipitate. When the pore solution is undersaturated with respect to a certain solid (saturation index < 0), this latter is not formed but may dissolve if present. The calculations show that three hydrate phases are oversaturated with respect to the pore solutions of TER-G or TER-A at any hydration time (Fig. 8), AFt, monosulphoaluminate and strätlingite (C_2ASH_8). Gibbsite (crystalline AH_3), which is oversaturated during early hydration, becomes undersaturated at later ages. Gypsum is always undersaturated. C-S-H and CH are oversaturated with respect to the pore solutions only at later ages.

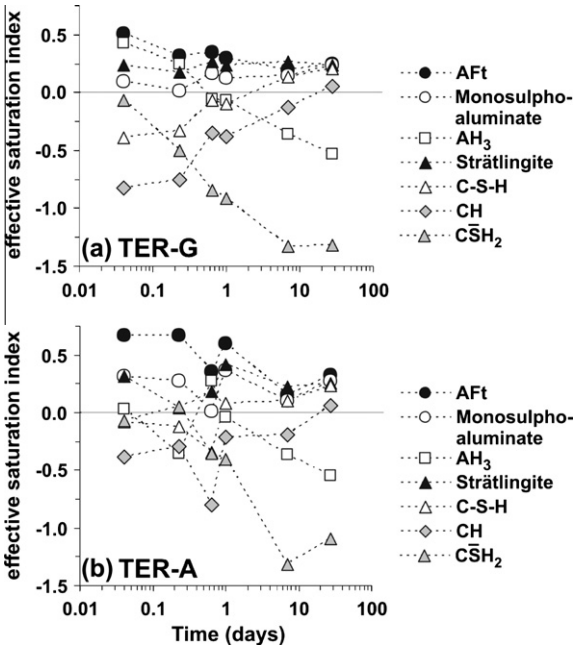

Fig. 8. Effective saturation indices calculated for the ettringite (AFt), monosulphoaluminate, AH_3 (gibbsite), strätlingite (C_2ASH_8), C-S-H (jennite), portlandite (CH) and gypsum ($C\bar{S}H_2$). An effective saturation index of 0 indicates the equilibrium between the liquid and the solid phases. Jennite is presented for C-S-H, while tobermorite would give a similar calculated trend.

The model predicts the formation of crystalline AH_3. This discrepancy between the model and the analytical data is due to the fact that the solubility product of AH_3 is strongly dependent on its crystallinity. At about 20 °C the amorphous AH_3 has a solubility product around $10^{-1.99}$ [41], the micro-crystalline AH_3 around $10^{-0.22}$ [42,43], and the crystalline AH_3 (gibbsite) around $10^{-0.06}$ [44]. In that case, the modelling program favours the formation of the component with the lowest solubility product, respectively gibbsite (according to the Ostwald step rule). Therefore in cement systems, amorphous or micro-crystalline AH_3 could form during early hydration and could be progressively recrystallized to more crystalline AH_3.

The calculation of the saturation indices allows a better estimation of the composition of the hydrates amorphous fraction present in TER-G and TER-A. In TER-G until 1 day, this component should be mainly composed of AH_3 and could contain some additional strätlingite (C_2ASH_8), explaining the Si content deduced from the mass balance calculations (Fig. 4a). At later ages, while the AH_3 content in the amorphous fraction decreases, a C-S-H type phase can be formed. This could easily explain the calculated decrease of the Al to Si ratio over time (Fig. 4a). Some monosulphoaluminate could also form, as the S content in the amorphous fraction increases at later ages (Fig. 4a). A similar scenario can be drawn for TER-A. However in that case, some strätlingite and some monosulphoaluminate could also form in the amorphous fraction within the first hour of hydration (Fig. 4b).

4.3.2. Hydration mechanism

The thermodynamic modelling is used to calculate the stable phase assemblage during the hydration based on the measured dissolution of the clinker phases (XRD/Rietveld refinement). The modelling reveals that the main differences between the hydration mechanisms of TER-G and TER-A occur within the first day. For that reason, the modelled compositions of the hydrated cements are presented until 7 days in Fig. 9. In TER-G, the hydration process begins with the formation of AFt and AH_3 from the hydration of $C_4A_3\bar{S}$, which is in agreement with the analytical data and with reaction (i) $C_4A_3\bar{S} + 2C\bar{S}H_2 + 34H \rightarrow C_3A{\cdot}3C\bar{S}{\cdot}H_{32} + 2AH_3$. The AFt content strongly increases during the first hours, then stays more or less constant, and finally decreases at later ages. This evolution is in agreement with the Rietveld refinement results (Fig. 2c). Some C-S-H and strätlingite are also modelled to form within the first hours. As these phases are not observed by XRD, they could be present in the hydrates amorphous fraction. This would explain the increase of the Si content shown in Fig. 4a within the first hours of hydration (mass balance calculation). Later, AH_3 content decreases and after 1 day monosulphoaluminate starts to form. According to the modelling, the composition of the monosulphoaluminate solid solution is close to the monosulphoaluminate end-member ($C_4A\bar{S}H_{12}$). As monosulphoaluminate is not observed by XRD (only suspected beyond 7 days), it could be present in the amorphous fraction, which is consistent with the increase of the S content from 1 day shown in Fig. 4a. No CH was predicted to form in the modelled hydration process.

Comparing the amorphous content calculated by XRD/Rietveld refinement to the total amount of amorphous phases calculated by the modelling, respectively those being absent from the XRD patterns, strätlingite, AH_3, C-S-H and monosulphoaluminate (Fig. 10), there is a good correlation between the Rietveld and the modelled results until 28 days. From this observation, we can conclude that these four phases belong to the hydrates amorphous fraction. Moreover, during early hydration of TER-G, the

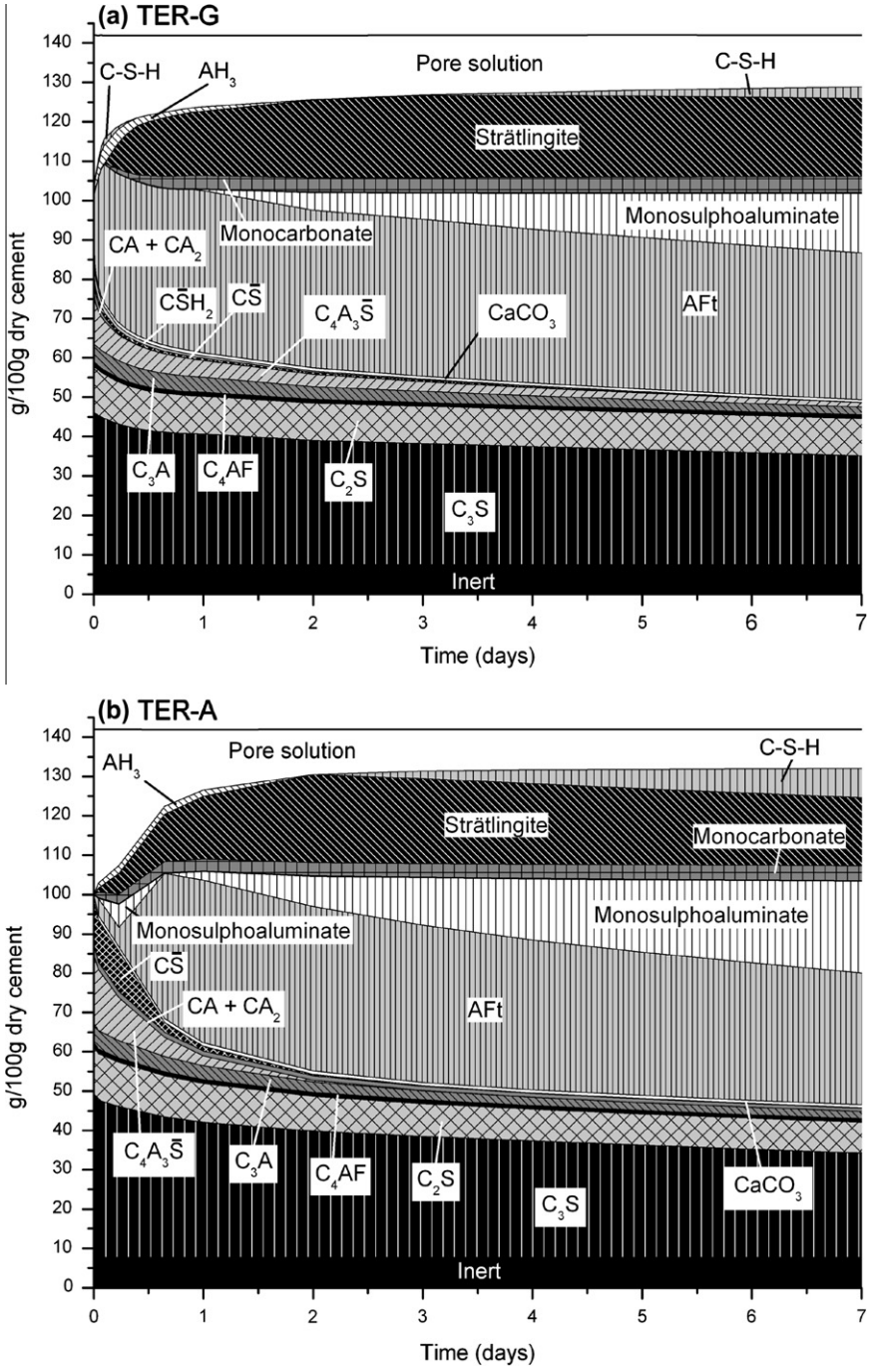

Fig. 9. Modelled hydration until 7 days of a) the gypsum-bearing system (TER-G) and b) of the anhydrite-bearing system (TER-A). Calculation made with w/c = 0.42 and 20 °C. Results expressed as mass in g/100 g dry cement. AFt = ettringite, AH_3 = gibbsite, CA = monocalcium aluminate, CA_2 = monocalcium dialuminate, C_3A = aluminate, C_4AF = ferrite, $C_4A_3\overline{S}$ = ye'elimite, $CaCO_3$ = calcite, C_3S = alite, C_2S = belite, $C\overline{S}$ = anhydrite, $C\overline{S}H_2$ = gypsum. Monosulphoaluminate is an SO_4–OH–monosulphate solid solution close to $C_4A\overline{S}H_{12}$. Inert includes the non hydraulic phases spinel (MA), CT, gehlenite (C_2AS) and SiO_2. C-S-H composition is a tobermorite–jennite solid solution close to the jennite endmember, except for TER-G at early age where some tobermorite-amorphous SiO_2 solid solution compositions were calculated (close to the tobermorite endmember). Hydrotalcite is present in both mixes and approximately constant at low concentrations (<0.16 g/100 g dry cement). As no CA_2 dissolution kinetics could be deduced from the Rietveld refinement, the empirical function of the CA dissolution was used to model the CA_2 decrease.

monosulphoaluminate is formed as one of the X-ray amorphous hydrates, which could at later ages increase its crystallinity.

In TER-A, little AFt is predicted to form within the first hour of hydration, while the period where the higher amount of AFt is formed is between 5 h 30 and 15 h 30 (Fig. 9b), which is in agreement with the Rietveld refinement results (Fig. 2d). The AFt content decreases at later ages. Monosulphoaluminate is predicted to form earlier in TER-A than in TER-G. This is certainly related to the slower dissolution of anhydrite compared to gypsum, as observed for CSA cements [8,29]. According to the modelling, AH_3 and strätlingite are formed during early hydration in addition to monosulphoaluminate (Fig. 9b). This easily explains the observed SiO_2 and SO_3 contents in the hydrates amorphous fraction at early age (mass balance calculations; Fig. 4b). The most significant discrepancies between the Rietveld refinement results and the modelling results are the absence of CH and the high amount of

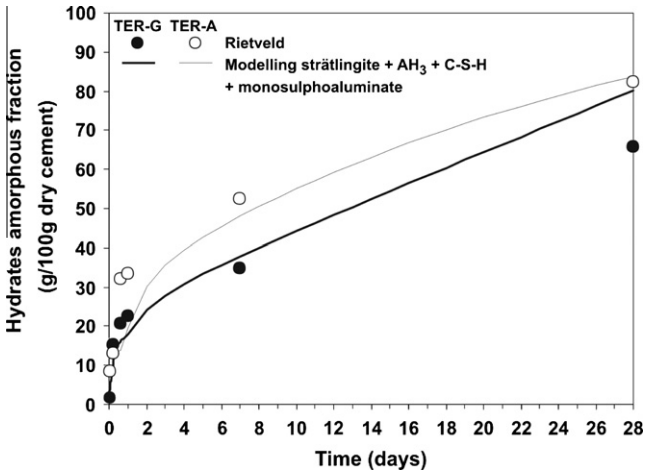

Fig. 10. Comparison between XRD/Rietveld refinement and modelled contents of X-ray amorphous hydrates over time in the gypsum-bearing system (TER-G) and anhydrite-bearing system (TER-A). Circles represent XRD/Rietveld refinement results and continuous lines represent the modelled content of strätlingite + AH_3 + C-S-H + monosulphoaluminate.

monosulphoaluminate calculated by GEMS. However as for TER-G, if the modelled amounts of monosulphoaluminate, strätlingite, AH_3 and C-S-H are considered to be part of the hydrates amorphous fraction, the correlation between the Rietveld results and the modelled results is good until 28 days (Fig. 10). From these observations we can conclude that, as for TER-G, the monosulphoaluminate is formed at early age as an X-ray amorphous hydrate which becomes more crystalline at later ages.

5. Conclusion

The combination of X-ray diffraction, Rietveld refinement and thermogravimetric analysis with the measurement of the composition of pore solutions over time allows a precise understanding of the hydration mechanism of OPC, CSA clinker and calcium sulphate ternary blends. The overall hydration mechanisms are similar in presence of gypsum or anhydrite, the main difference being in the kinetics of reactions due to the slower dissolution of anhydrite compared to gypsum in the presence of sodium gluconate, which was added as retarding agent to achieve fluidity for sample casting. The hydration starts with the formation of some ettringite and of some X-ray amorphous hydrates, while ye'elimite, calcium sulphate and alite contents are decreasing. In the anhydrite-bearing system, the ettringite-forming reaction is strongly delayed by the addition of the sodium gluconate compared to the gypsum-bearing system where it is only slightly delayed. This results in the formation of an important amount of X-ray amorphous hydrates before the ettringite starts to form in the anhydrite-bearing system. At later ages, the ettringite content decreases in the ternary binders, while some portlandite is formed. The volume of the hydrates amorphous fraction present in the two ternary binders constantly increases.

From the successful combination of the results obtained on the solid and liquid phases with thermodynamic modelling, the composition of the hydrates amorphous fraction observed in the ternary binders can be efficiently estimated. The mass ratio between the phases present in the X-ray amorphous fraction changes over time. In the gypsum-bearing and anhydrite-bearing systems, the Al to Si ratio of the amorphous fraction decreases over time. Within the first hours, the hydrates amorphous fraction is mainly composed of aluminium hydroxide and strätlingite, while in the anhydrite-bearing system it can additionally contain some monosulphoaluminate due to the slower consumption of anhydrite compared to gypsum. At later ages, the aluminium hydroxide content in the amorphous fraction decreases and additional monosulphoaluminate and a C-S-H type phase are formed.

Acknowledgements

The authors would like to thank the innovation promotion agency (CTI) in Switzerland for its financial support (Project no. 9623.1; 3 PFIW-IW) and the Saint Gobain Weber Favo research teams. Thanks are extended to L. Brunetti and A. Steffen for their experimental support in the laboratory.

References

[1] Palou M, Majling J, Janotka I. The performances of blended cements based on sulfoaluminate belite and Portland cements. In: Grieve G, Owens G, editors. Proceedings 11th ICCC. Durban: The Cement and Concrete Institute of South Africa; 2003. p. 1896–02.
[2] Cau Dit Coumes C, Courtois S, Peysson S, Ambroise J, Pera J. Calcium sulfoaluminate cement blended with OPC: A potential binder to encapsulate low-level radioactive slurries of complex chemistry. Cem Concr Res 2009;39:740–7.
[3] Pelletier L, Winnefeld F, Lothenbach B. Hydration mechanism and strength development of the ternary Portland cement–calcium sulfoaluminate cement–anhydrite. 17. Internationale Baustofftagung (ibausil), Weimar, Germany, vol. 1. 2009, p. 277–82.
[4] Pelletier L, Winnefeld F, Lothenbach B. The ternary system Portland cement–calcium sulphoaluminate clinker–anhydrite: hydration mechanism and mortar properties. Cem Concr Comp 2010;32:497–507.
[5] Taczuk L, Bayoux JP, Sorrentino F, Capmas A. Understanding of the hydration mechanisms of C_4A_3S–Portland clinker–$CaSO_4$ mixes. In: Mullick AK, editor. Proceedings 9th ICCC. New Delhi: National Council for Cement and Building Materials; 1992, p. 278–84.
[6] Locher FW, Richartz W, Sprung S. Erstarren von Zement. Teil II: Einfluss des Calciumsulfatzusatzes. Zement Kalk Gips 1980;33:271–7.
[7] Glasser FP. Advances in sulfoaluminate cements. In: Proceedings 5th int symp on the cement and concrete, vol. 1, 2002. p. 14–24.
[8] Winnefeld F, Barlag S. Influence of calcium sulfate and calcium hydroxide on the hydration of calcium sulfoaluminate clinker. ZKG Int 2009;12:42–53.
[9] Winnefeld F, Barlag S. Calorimetric and thermogravimetric study on the influence of calcium sulfate on the hydration of ye'elimite. J Therm Anal Calorim 2010;101(3):949–57.
[10] Franke A. Bestimmung von Calciumoxid und Calciumhydroxid neben wasserfreiem und wasserhaltigem Calciumsilikat. Z Anorg Allg Chem 1941;247:180–4.
[11] Lothenbach B, Winnefeld F. Thermodynamic modelling of the hydration of Portland cement. Cem Concr Res 2006;36:209–26.
[12] Wadsö L. Applications of an eight-channel isothermal conduction calorimeter for cement hydration studies. Cem Int 2005;5:94–101.
[13] Le Saout G, Kocaba V, Scrivener K. Application of the Rietveld method to the analysis of anhydrous cement. Cem Concr Res 2011;41:133–48.
[14] Calos NJ, Kennard CHL, Whittaker AK, Davis RL. Structure of calcium aluminate sulfate $Ca_4Al_6O_{16}S$. J Solid State Chem 1995;119:1–7.
[15] Saalfeld H, Depmeier W. Silicon-free compounds with sodalite structure. Kristall Technik 1972;7:229–33.
[16] Swainson IP, Dove MT, Schmahl WW, Putnis A. Neutron diffraction study of the akermanite–gehlenite solid solution series. Phys Chem Miner 1992;19:185–95.
[17] Hoerkner W, Mueller-Buschbaum H. Zur Kristallstruktur von $CaAl_2O_4$. J Inorg Nucl Chem 1976;38:983–4.
[18] Ponomarev VI, Kheiker DM, Belov NV. Crystal structure of calcium dialuminate, CA_2. Kristallografiya 1970;15:1140–3.
[19] Sasaki S, Prewitt CT, Bass JD. Orthorhombic perovskite $CaTiO_3$ and $CdTiO_3$: structure and space group. Acta Crystallogr C 1987;43:1668–74.
[20] Finger LW, Hazen RM, Hofmeister AM. High-pressure crystal chemistry of spinel ($MgAl_2O_4$) and magnetite (Fe_3O_4): comparison with silicate spinels. Phys Chem Miner (Germany) 1986;13:215–20.
[21] Jenkins R, Snyder RL. Introduction to X-ray Powder Diffractometry. In: Winefordner JD, editor. Chemical analysis. A series of monographs on analytical chemistry and its application. New York; 1996. 404p.
[22] Taylor HFW. Cement chemistry. London: Academic Press, Harcourt Brace Jovanovich Publishers; 1990.
[23] Hummel W, Berner U, Curti E, Pearson FJ, Thoenen T., Nagra/PSI chemical thermodynamic data base 01/01, Universal Publishers/uPUBLISH.com, USA, also published as Nagra Technical Report NTB02 16, Wettingen, Switzerland; 2002.
[24] Thoenen T, Kulik D. Nagra/PSI chemical thermodynamic database 01/01 for the GEM-Selektor (V.2-PSI) geochemical modelling code, PSI, Villigen; 2003. <http://gems.web.psi.ch/doc/pdf/TM-44-03-04-web.pdf>.

[25] Matschei T, Lothenbach B, Glasser FP. Thermodynamic properties of Portland cement hydrates in the system $CaO–Al_2O_3–SiO_2–CaSO_4–CaCO_3–H_2O$. Cem Concr Res 2007;37:1379–410.
[26] Lothenbach B, Matschei T, Möschner G, Glasser FP. Thermodynamic modelling of the effect of temperature on the hydration and porosity of Portland cement. Cem Concr Res 2008;38:1–18.
[27] Kulik D. GEMS 2.3 software. PSI Villigen, Switzerland; 2009. <http://gems.web.psi.ch/download/reposit/selpack.html>.
[28] Longuet P, Burglen L, Zelwer A. La phase liquide du ciment hydraté. Revue des Matériaux de Construction 1973;676:35–41.
[29] Winnefeld F, Lothenbach B. Hydration of calcium sulfoaluminate cements–experimental findings and thermodynamic modelling. Cem Concr Res 2010;40:1239–47.
[30] Andac M, Glasser FP. Pore solution composition of calcium sulfoaluminate cement. Adv Cem Res 1999;11(1):23–6.
[31] Hong S-Y, Glasser FP. Alkali binding in cement pastes. Part I. The C-S-H phase. Cem Concr Res 1999;29:1893–903.
[32] Hong S-Y, Glasser FP. Alkali sorption by C-S-H and C–A–S–H gels. Part II. Role of alumina. Cem Concr Res 2002;32:1101–11.
[33] Brew DMR, Glasser FP. The magnesia-silica gel phase in slag cements: alkali (K, Cs) sorption potential of synthetic gels. Cem Concr Res 2005;35:77–83.
[34] Garcia Lodeíro I, Fernández-Jimenez A, Palomo A, Macphee DE. Effect on fresh C-S-H gels of the simultaneous addition of alkali and aluminium. Cem Concr Res 2010;40:27–32.
[35] Lothenbach B, Le Saout G, Gallucci E, Scrivener K. Influence of limestone on the hydration of Portland cements. Cem Concr Res 2008;38:848–60.
[36] Plank J, Chatziagorastou P, Hirsch C. New model describing distribution of adsorbed superplasticizer on the surface of hydrating cement grain. J Build Mater 2007;10:7–13.
[37] Plank J, Keller H, Yu B. Conditions determining the formation of organo-mineral phases in concrete. In: Holland TC, Gupta PR, Malhotra VM, editors. Ninth ACI international conference on superplasticizers and other chemical admixtures in concrete, supplementary papers. Sevilla; 2009. p. 235–56.
[38] Plank J, Hirsch C. Impact of zeta potential of early cement hydration phases on superplasticizer adsorption. Cem Concr Res 2007;37:537–42.
[39] Zingg A, Winnefeld F, Holzer L, Pakusch J, Becker S, Gauckler L. Adsorption of polyelectrolytes and its influence on the rheology, zeta potential, and microstructure of various cement and hydrate phases. J Colloid Interf Sci 2008;323:301–12.
[40] Zingg A, Holzer L, Kaech A, Winnefeld F, Pakusch J, Becker S, et al. The microstructure of dispersed and non-dispersed fresh cement pastes – New insight by cryo-microscopy. Cem Concr Res 2008;38:522–9.
[41] Atkins M, Bennett DG, Dawes AC, Glasser FP, Kindness A, Read D. A thermodynamic model for blended cements. Cem Concr Res 1992;22:497–502.
[42] Percival A, Taylor HFW. Monocalcium Aluminate Hydrate in the System $CaO–Al_2O_3–H_2O$ at 21 C. J Chem Soc 1959;526:2629–31.
[43] Faurie-Mounier MT. Contribution à l'étude du système $CaO–Al_2O_3–H_2O$. Revue des Matériaux Cimentaires 1966;635–636:305–12.
[44] Bennett DG, Read D, Atkins M, Glasser FP. A thermodynamic model for blended cements: II: Cement hydrate phases; thermodynamic values and modelling studies. J Nucl Mater 1992;190:315–25.